Applied Physics Letters ARTICLE scitation.org/journal/apl

# Energy barriers for Dy and H penetrating graphene on 6*H*-SiC(0001) and freestanding bilayer graphene from first-principles calculations

Cite as: Appl. Phys. Lett. **119**, 033101 (2021); doi: 10.1063/5.0056916
Submitted: 15 May 2021 · Accepted: 7 July 2021 ·
Published Online: 20 July 2021



Yong Han,[a] James W. Evans, and Michael C. Tringides

## AFFILIATIONS

Ames Laboratory, U.S. Department of Energy, Ames, Iowa 50011, United States and Department of Physics and Astronomy, Iowa State University, Ames, Iowa 50011, United States

[a]Author to whom correspondence should be addressed: y27h@ameslab.gov

## ABSTRACT

Currently, intercalation of foreign guest atoms into two-dimensional (2D) layered van der Waals materials is an active research area motivated in part by the development of next-generation energy-storage technologies and optoelectronic devices. One such extensively studied 2D material is the graphene-on-SiC system. To realize and control the desired intercalated structures, it is fundamentally important to understand the kinetic process of intercalation. For the intercalation of a guest atom into graphene layers on SiC substrate, a critical kinetic parameter is the energy barrier of a guest atom penetrating the perfect graphene top layer into the gallery under it. However, accurate theoretical calculations for such penetration barriers are unavailable in literature. From our first-principles density functional theory calculations, we obtain the global energy barriers of 3.47 and 1.80 eV for single Dy and H atoms penetrating the graphene top layer on a graphene buffer layer supported by a Si-terminated 6*H*-SiC(0001) substrate, respectively. For comparison as well as for examining the lateral strain effects, we also obtain the global barriers of 5.05 and 1.50 eV for single Dy and H atoms penetrating freestanding bilayer graphene with a tensile strain of about 8.8% to match our model for supported graphene, as well as the global barriers of 7.21 and 4.18 eV for penetrating unstrained freestanding bilayer graphene, respectively. From corresponding minimum energy paths with multiple energy minima and saddle points, we can also obtain various local energy barriers and the global backward barrier from the graphene gallery back to the top surface.



Intercalation of foreign guest atoms into two-dimensional (2D) layered van der Waals (vdW) materials is becoming a rapidly growing research area for developing next-generation energy-storage technologies and optoelectronic devices.[1–3] An extensively reported example is intercalation of various guest atoms into the epitaxial graphene supported by an SiC substrate.[4] As a result of intercalation under the so-called buffer layer graphene, graphene can be decoupled from the SiC substrate to consequently obtain desirable quasi-freestanding graphene layers.[5–9] Many new interesting and important properties from these intercalation studies have also been reported, such as superconductivity,[10–15] high-performance graphene transistors,[16] quantum Hall effect,[17] band structure tuning,[18–21] metal-dielectric transitions,[22] semiconductor to metal transitions,[23] etc.

To realize relevant promising applications, an understanding of the kinetics of the intercalation process is fundamentally important. A key parameter that must be considered for controlling the kinetic process of intercalation is the energy barrier of a guest atom penetrating the perfect top graphene layer into the gallery underneath it. However, appropriate theoretical assessment of such a critical energy parameter, especially from density functional theory (DFT) plus the climbing image nudged elastic band (CINEB) method,[24] appears to be lacking. Note that the DFT-plus-CINEB method for calculating minimum energy paths (MEPs) and consequently for obtaining the diffusion barriers is well-developed and more reliable relative to the earlier methods.[24] To estimate the penetration barriers of alkali atoms (Li, Na, Rb, and Cs) into graphene on SiC, Boukhvalov *et al.*[25] constructed a rough model using a bilayer graphene with a partially hydrogenated bottom graphene as the artificial buffer-layer graphene (BLG) between the top-layer graphene (TLG) and terminal Si layer of a SiC substrate, i.e., the model is not a real graphene-on-SiC system. In addition, their DFT calculations do not involve the CINEB method.

In this Letter, we report the first-principles DFT-plus-CINEB results for energy barriers of single guest Dy and H atoms penetrating graphene supported on a 6*H*-SiC(0001) substrate. For the graphene-SiC system, we consider two graphene layers above the terminal Si layer of the SiC substrate: specifically the TLG and the underlaying BLG. We

choose the typical rare-earth element Dy, as experiments show that intercalation occurs,[26] and also choose H for which multiple studies are reported in the literature.[5,9,16,17,27–35] For the 6*H*-SiC(0001) substrate, previous experiments suggest that supported graphene layers exhibit $(6\sqrt{3} \times 6\sqrt{3})R30°$ superlattice ordering,[36,37] which evolves at lower temperatures from superstructures including the $(\sqrt{3} \times \sqrt{3})R30°$ superlattice ordering.[36] Thus, for DFT calculations, there are two reasonable models for describing the graphene-SiC system. In model 1, a $13 \times 13$ graphene overlayer with a small lateral tensile strain of about 0.4% matches the substrate, while a $2 \times 2$ graphene overlayer with a relatively larger lateral tensile strain of about 8.8% matches the substrate in model 2.[38] Due to the extreme computational expense for model 1, we only choose model 2, which, in fact, has already been widely used in literature.[9,39–42] However, to examine the strain effects and the substrate effects, we also report our results for penetration into unsupported or freestanding bilayer graphene with and without a tensile strain of about 8.8%. The former matches the strain in the supported graphene. Results for intercalation through freestanding bilayer graphene are also instructive, given recent experiments for K, Cs, Li, and Pd intercalations in freestanding bilayer graphene.[43] The DFT method used in this work was described previously in detail,[38] and key information is provided in the supplemental material.

To obtain the MEP of a guest atom penetrating the top graphene layer into the underlying gallery for both supported and unsupported graphene, we first need to find two appropriate configurations as the CINEB endpoints. For these, the guest atom is either adsorbed on TLG or intercalated in the gallery between the two graphene layers (the TLG and the BLG in the supported case). By relaxing the configurations with the guest atom initially at seven different positions (see Fig. 1) for both adsorption and intercalation, we can find various local equilibrium configurations.[44]

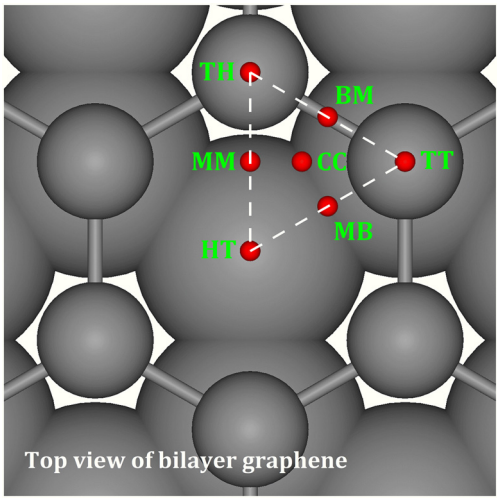


**FIG. 1.** Top view of bilayer graphene with a guest atom at seven different positions (red dots) considered in our DFT calculations for adsorption and intercalation. Small (large) balls represent the top (bottom) graphene layer. The letters T, H, M, B, and C stand for top, hollow, midpoint, bridge, and center, respectively. The first (second) letter corresponds to the top (bottom) graphene layer. An additional letter "t (i)" will be used to indicate adsorbed top (intercalated) positions.

First, we present results for intercalation of a guest Dy atom. We find that the energetically most favorable adsorption position is always at a tHT site (where "t" labels the guest atom on top), which is taken as our first CINEB endpoint. The second endpoint is taken to be a local energy minimum, where the Dy atom is intercalated in the gallery with the shortest distance from the Dy atom for the first endpoint. We find that this second endpoint is always approximately at iHT (where "i" labels the guest atom in the gallery). Using these two endpoints, we perform CINEB calculations for three systems and obtain the MEPs in Fig. 2. The binding energy for the guest Dy atom shown in Fig. 2 is defined as $E_{bind} = E_{tot} - E_{cln} - E_{gas}$, where $E_{tot}$ is the total energy of the guest atom plus graphene supported on SiC or plus freestanding graphene, $E_{cln}$ is the energy of the clean graphene-SiC or freestanding graphene system without the guest atom, and $E_{gas}$ is the energy of the guest atom in the gas phase. As seen in Fig. 2, an MEP can have multiple energy minima and saddle points. We denote the energy minima as m*i*, where $i = 0, 1, 2, \ldots$, starting from the first endpoint m0, and the saddle points as s*j*, where $j = 1, 2, 3, \ldots$, from adsorption toward intercalation along the MEP. The binding energies corresponding to m*i* and s*j* are listed in Table I, from which any local energy barrier can be readily calculated by taking the energy difference between m*i* and s*j* by specifying *i* and *j*. The global barrier for penetration is the energy of the highest saddle point relative to m0, as indicated in bold font in Table I and by the blue arrows in Fig. 2. In addition, because $E_{bind}$ at a tHT site (m0 in Fig. 2) is always lower than that at an iHT site [m3 in Fig. 2(a), m2 in Fig. 2(b), and m3, m4, m5, or m6 in Fig. 2(c)], the intercalation into the gallery is always energetically more favorable than the adsorption on the top.[38,44]

For the graphene-SiC system in Fig. 2(a), we find three saddle points. The highest one is s2 corresponding to the global barrier of 3.47 eV. For the freestanding bilayer graphene with the same tensile strain (about 8.8%) as that in Fig. 2(a) (i.e., after removing SiC), we find two saddle points with s1 corresponding to a larger global barrier of 5.05 eV, indicating that the SiC substrate reduces the penetration barrier by 1.58 eV. In addition, the SiC substrate also changes the intercalation details, e.g., during the penetration, some C atoms near the Dy atom are pushed down to the gallery in Fig. 2(a), but up to the top in Fig. 2(b), as shown in the trajectories. This indicates that the SiC substrate has significant interactions with the C atoms of the graphene above it.

For the unstrained bilayer graphene in Fig. 2(c), we do not find a short direct intercalation pathway, in contrast to Fig. 2(a) or Fig. 2(b), where the Dy atom directly goes down to the gallery. Instead, we find that the Dy atom first sequentially pushes two nearby C atoms up and then goes down to the gallery, as illustrated by the trajectory in Fig. 2(c). The global barrier of 7.21 eV appearing at s3 is significantly larger than 5.05 eV for the strained graphene in Fig. 2(b). This indicates the difficulty of penetrating an unstrained graphene layer. That exerting a tensile strain can significantly change the MEP and reduce the penetration barrier is likely due to the increased graphene lattice constant from $a_C = 2.465$ Å to $a_C^* = 2.681$ Å, for which the area of a $C_6$ ring becomes larger and, therefore, provides a wider space for an easier penetration. For a complementary analysis from the electron localization function (ELF)[46] plots, see the discussion for Fig. S1 in the supplementary material. Additionally, we also obtain a barrier of 0.09 eV for the Dy atom diffusing within the gallery for unstrained graphene, as plotted in Fig. 2(c), where m3 corresponds to the final configuration of the trajectory, and m6 corresponds to the Dy atom at an iHT site close

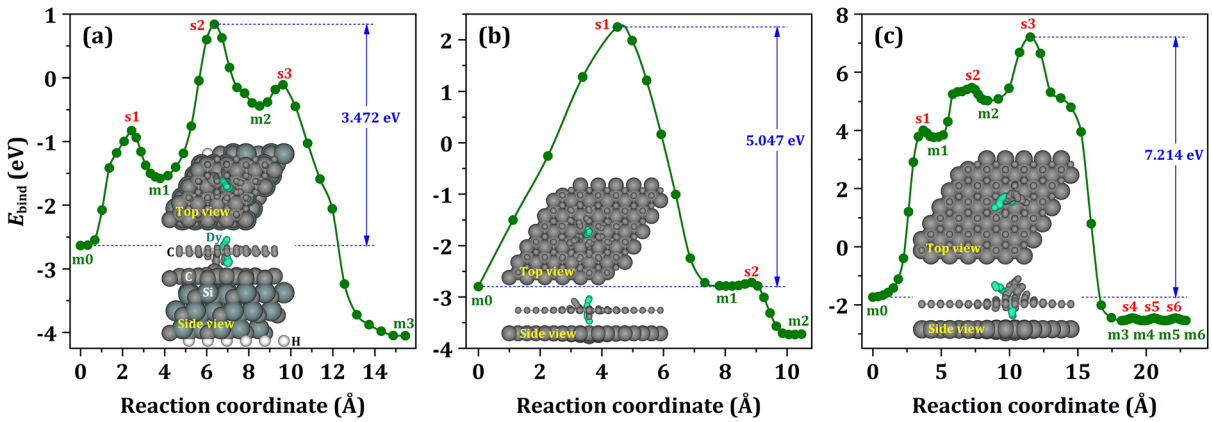


**FIG. 2.** MEPs (green curves) of a Dy atom penetrating graphene. (a) Supported $4a_C^* \times 4a_C^*$ TLG plus BLG matching $2\sqrt{3}a_{SiC} \times 2\sqrt{3}a_{SiC}$ Si-terminated 6*H*-SiC(0001) substrate, where $a_C^* = 2.681$ Å is the lattice constant of graphene with a tensile strain of about 8.8% relative to the SiC(0001) lattice constant $a_{SiC} = 3.095$ Å.[38] (b) Freestanding $6a_C^* \times 6a_C^*$ bilayer graphene with a tensile strain of about 8.8%. (c) Freestanding unstrained $6a_C \times 6a_C$ bilayer graphene, where $a_C = 2.465$ Å.[45] Green dots on the curves are the CINEB images. Insets show the trajectories for the Dy penetrations and also indicate the supercells with top and side views. To avoid the possible lateral shift of TLG during relaxation,[38] we fix the lateral coordinates of one C atom far from the Dy atom for each graphene layer. For (a), the *k* mesh is $6 \times 6 \times 1$, and the dangling bonds of bottommost C atoms are passivated by pseudo-H atoms. For (b) and (c), *k* mesh is $4 \times 4 \times 1$.

to and below the initial tHT site at m0. The diffusion path m3 → s3 → m4 → s4 → m5 → s5 → m6 is composed of three identical hops due to the geometric symmetry, and not included in the trajectory in Fig. 2(c). Thus, the entire MEP from m0 to m6 in Fig. 2(c) is a rather detoured pathway, in contrast to Figs. 2(a) and 2(b), again indicating the difficulty of the Dy atom penetrating an unstrained graphene layer.

As mentioned above, overlayer graphene for model 1 has a negligible strain of about 0.4%, close to an unstained graphene. Therefore, we expect that the penetration barrier $E_{dp}$ for model 1 is likely significantly larger than 3.47 eV for model 2 in Fig. 2(a), but not greater than 7.21 eV for unstrained graphene in Fig. 2(b) by considering that the graphene can relax and consequently result in significant corrugations, so that the local tensile strain larger than 0.4% is likely available.[38] Thus, we obtain a lower limit of 3.47 eV and an upper limit of 7.21 eV for a Dy atom penetrating any graphene-SiC system. Consider the penetration rate with the Arrhenius forms $r_{dp} = \nu e^{-E_{dp}/(k_B T)}$, where $\nu \approx 10^{13}$/s is the attempt frequency, $T$ is the temperature, and $k_B$ is the Boltzmann constant. For $E_{dp} = 3.47$ to

**TABLE I.** DFT data (also see TABLE S2 in the supplemental material for expended decimal digits) for binding energy $E_{bind}$ and relative energy (in eV) for energy minima m*i* and saddle points s*j* in Fig. 2 for Dy and Fig. 3 for H.

| | Configuration | Fig. 2(a) | Fig. 2(b) | Fig. 2(c) | Fig. 3(a) | Fig. 3(b) | Fig. 3(c) |
|---|---|---|---|---|---|---|---|
| Binding energy | m0 | −2.63 | −2.80 | −1.74 | −1.92 | −1.78 | −0.97 |
| | s1 | −0.83 | 2.25 | 4.01 | −0.14 | −0.42 | 3.21 |
| | m1 | −1.58 | −2.79 | 3.76 | −0.17 | −0.50 | −0.90 |
| | s2 | 0.84 | −2.72 | 5.48 | −0.13 | −0.28 | |
| | m2 | −0.44 | −3.73 | 5.03 | −1.69 | −1.76 | |
| | s3 | −0.11 | | 7.21 | −0.69 | | |
| | m3 | −4.05 | | −2.54 | −2.98 | | |
| | s4, s5, s6 | | | −2.46 | | | |
| | m4, m5, m6 | | | −2.54 | | | |
| Relative energy | m0 | 0.00 | 0.00 | 0.00 | 0.00 | 0.00 | 0.00 |
| | s1 | 1.80 | **5.05** | 5.75 | 1.78 | 1.36 | **4.18** |
| | m1 | 1.05 | 0.01 | 5.50 | 1.75 | 1.28 | 0.07 |
| | s2 | **3.47** | 0.08 | **7.21** | **1.80** | **1.50** | |
| | m2 | 2.19 | −0.93 | 6.77 | 0.23 | 0.01 | |
| | s3 | 2.52 | | 8.95 | 1.23 | | |
| | m3 | −1.42 | | −0.81 | −1.06 | | |
| | s4, s5, s6 | | | −0.72 | | | |
| | m4, m5, m6 | | | −0.81 | | | |

7.21 eV and an experimental annealing temperature up to $T = 900\,^{\circ}\mathrm{C}$,[26] the rate $r_{dp} = 10^{-2}$ to $10^{-18}$/s, which is very low for the penetration. This has motivated us to consider other pathways which might be operative to interpret the experimentally observed intercalation for this system.[38]

From the MEP in Fig. 2(a), we also note that there is a barrier $E_{m0\to m1}$ (at s1) from m0 to m1. If $E_{m0\to m1}$ is not sufficiently high, the energy of m1 is sufficiently low (e.g., lower than m0), and s2 is sufficiently high, then m1 is a rather stable configuration corresponding to a guest-atom-induced TLG point defect, where a C atom is pushed down by the guest atom (plus the SiC substrate effect described above) to form a $sp^3$-like hybridization with a C atom in the BLG. In Fig. 2(a), $E_{m0\to m1} = 1.80$ eV and s2 is sufficiently high, but m1 is not sufficiently low with a relatively small local backward barrier $E_{m1\to m0} = 0.75$ eV. Thus, it is not quite possible for a Dy atom to induce a defect within a temperature range of interest in experiments. However, we do not rule out that another type of guest atom can simultaneously satisfy the above three conditions so that the guest-atom-induced point defects form in the TLG.

Next, we switch to consideration of intercalation of H guest atoms. Before discussing H penetration, let us first analyze the favorability of a single H atom on TLG and in the gallery underneath it. For the graphene-SiC system, we find that the most favorable adsorption position on TLG is at a tTT site (see m0 and trajectories) in Fig. 3(a). Unlike a metal atom (like Dy) generally ionically binding with its surrounding C atoms, the binding of a H atom is covalent with one nearby C atom.[44] As shown in Fig. 3(a), the iTT site of a H atom near TLG corresponds to a local minimum m2, and the most favorable site is at m3 with the H atom approximately at an iHT site near BLG. $E_{bind}$ at m2 is 0.23 eV higher than m0, while $E_{bind}$ at m3 is 1.06 lower than m0, indicating that the intercalation at m3 is much more favorable than at m0.

For freestanding bilayer graphene, the most favorable adsorption position on TLG is at a tTH site (see m0 and trajectories) in Figs. 3(b) and 3(c). There are two most favorable and identical binding sites in the gallery: one is at an iTH site near the TLG [i.e., m2 in Fig. 3(b) or m1 in Fig. 3(c)] and another one is its symmetric site iHT near the bottom-layer graphene. Although an energy barrier is expected between these two symmetric sites, we do not consider the H diffusion between them in this work. In addition, we find that $E_{bind}$ at m2 in Fig. 3(b) or m1 in Fig. 3(c) is higher than m0 by tens of meV (also see Table I), indicating that intercalation of a single H atom is more unfavorable than adsorption on TLG. Also, the $E_{bind}$ difference from top to gallery reduces from 0.07 eV to 0.01 eV after the strain is exerted from Fig. 3(c) to Fig. 3(b), indicating that the tensile strain can weaken the unfavourability of intercalation for freestanding bilayer graphene.

Using the above-obtained m*i* as the CINEB endpoints, we obtain the MEPs in Fig. 3. There is a similarity in the MEPs and trajectories from m0 to m2 in Figs. 3(a) and 3(b), where the H atom goes around a C atom from the tTT or tTH site (m0) to the iTT or iTH site (m2) through a BM site (see Fig. 1) as a local minimum m1. Thus, there appear two saddle points s1 and s2 from m0 to m2, the highest s2 corresponding to the global penetration barriers of 1.80 eV and 1.50 eV for strained graphene with and without SiC substrate, respectively. For an unstrained bilayer graphene, only one saddle point s1 with a larger penetration barrier of 4.18 eV is found, and the diffusion path goes through a MM site (see Fig. 1) approximately, as shown in Fig. 3(c). In contrast to Fig. 3(c), going through a BM site but not a MM site on the diffusion path with the significantly smaller global penetration barriers in Figs. 3(a) and 3(b) indicates that the tensile strain makes the penetration easier likely due to the expanded graphene lattice constant. For a complementary analysis from the ELF plots, see the discussion for Fig. S2 in the supplementary material. Additionally, using m2 and m3 in Fig. 3(a) as two CINEB endpoints, we obtain the partial MEP in Fig. 3(a) from m2 to s3 to m3. The energy difference from m3 to s3 gives a barrier of 2.29 eV for a H atom diffusing in the gallery. This large barrier indicates the strong bonding between the H atom and its adjacent C atom but is not related to penetration and will be discussed elsewhere.[47]

As analyzed above for Fig. 3(a), we obtain a global penetration barrier of 1.80 eV, which can be viewed as the lower limit of $E_{dp}$, considering that this result is obtained from a strained graphene layer on SiC (i.e., model 2). For almost-unstrained graphene on SiC (i.e., model 1), we estimate an upper limit of 4.18 eV from the freestanding unstrained bilayer graphene in Fig. 3(c) by, again, considering that the overlayer graphene can be locally tensile-strained due to the relaxation.

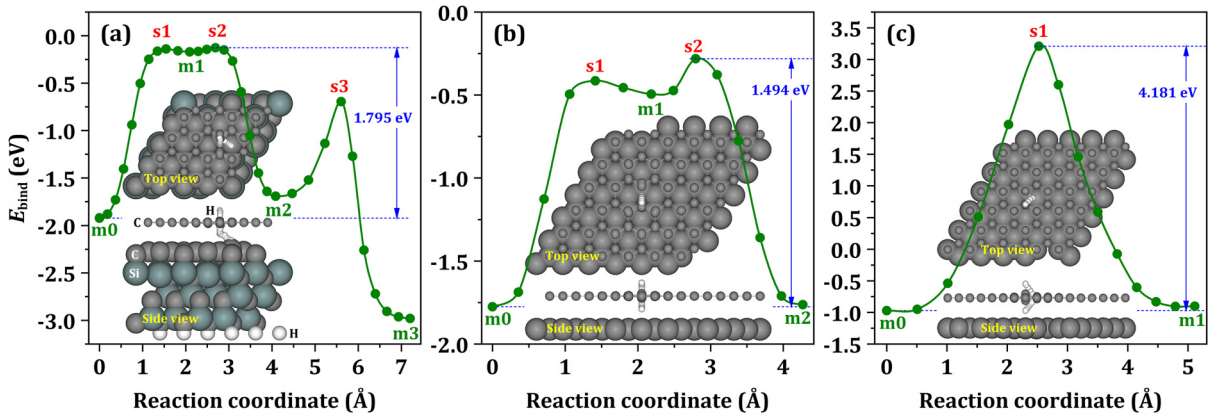


**FIG. 3.** MEPs of a H atom penetrating (a) supported $4a_C^* \times 4a_C^*$ TLG plus BLG on $2\sqrt{3}a_{SiC} \times 2\sqrt{3}a_{SiC}$ Si-terminated 6*H*-SiC(0001) substrate, (b) freestanding $6a_C^* \times 6a_C^*$ bilayer graphene with a strain of about 8.8%, and (c) freestanding unstrained $6a_C \times 6a_C$ bilayer graphene. Other details are similar to those in the caption of Fig. 2.

In experiments of Lin *et al.*,[33] the temperature for H intercalation into graphene on 6*H*-SiC(0001) substrate is higher than 700 °C. In experiments of Kunc *et al.*,[34] the H intercalation temperature for graphene on 4*H*-SiC(0001) substrate is 790 to 1510 °C. If we take the lower limit $E_{dp} = 1.80$ eV and $T = 790$ °C, then the penetration rate $r_{dp} = \nu e^{-E_{dp}/(k_B T)} = 3.1 \times 10^4$/s, which is sufficiently high for the penetration. Thus, the above $E_{dp}$ is reasonably consistent with the experimental H intercalation temperatures. Here, we need to mention that the nuclear quantum effects (NQEs) (including zero-point motion, discrete vibrational levels, and tunneling),[48,49] which are not taken into account in the calculations of this work, may affect the diffusion barriers for lightweight H. However, based on the above quantitative consistency analysis with experimental data, we reasonably expect that the NQEs would be not significant[50] at an experimentally typical intercalation temperature (much higher than 100 K). For instance, previous path-integral molecular dynamics calculations for diffusion of hydrogen isotopes in metals give a barrier modification of about tens of meV after considering NQEs above 60 K,[49] while the quantum tunneling effects for H on surfaces at the above intercalation temperatures can be generally negligible (for more information, see Sec. S4 in the supplementary material).

Finally, we also mention that reversible deintercalation of intercalated H is of relevance for potential technological applications, e.g., hydrogen storage.[5,27,28] For deintercalation of H, the key energy parameter is the backward barrier $E_{db}$ from the gallery to the top. The global backward barrier for each system in Fig. 2 or Fig. 3 can be obtained by taking the energy difference from the global minimum in the gallery to the highest saddle point. For example, using Table I, we get $E_{db} = 2.85$ eV by taking the energy difference from m3 to s2 in Fig. 3(a), and then the backward rate $r_{db} = \nu e^{-E_{db}/(k_B T)} \approx 5.5$/s at 900 °C, which is sufficiently high so that the intercalated H can be deintercalated.[5,27,28,35]

In conclusion, we have performed DFT-CINEB calculations and obtained the MEPs for single Dy and H atoms penetrating the graphene supported on 6*H*-SiC(0001) substrate and the freestanding bilayer graphene. The global energy barriers are 3.47 eV and 1.80 eV for the single Dy and H atoms penetrating graphene supported on the SiC substrate with the graphene having a strain of about 8.8%, respectively. For comparison, we also obtain the global penetration barriers of 5.05 eV and 1.50 eV for the Dy and H atoms after removing the SiC substrate but retaining strain, as well as 7.21 eV and 4.18 eV for penetrating the unstrained freestanding bilayer graphene, respectively. These results indicate that tensile strain can effectively reduce penetration barriers. Thus, we expect that the global energy barrier of a Dy atom penetrating realistic (locally almost-unstrained or strained) graphene on a SiC substrate is within 3.47 to 7.21 eV, and within 1.80 to 4.18 eV for a H atom. Recall that such a realistic system is so large that calculations for it are extremely demanding, and thus unavailable. From the binding energies (Table I) on corresponding MEPs, the specific local energy barriers and global backward barriers can be also obtained. The method used in this work applies for other types of guest atoms penetrating a 2D material.

See the supplementary material for the DFT method and benchmark analysis, DFT data with extended decimal digits, ELF plots for single Dy and H atoms plus freestanding bilayer graphene with and without tensile strain, and quantum tunneling information for H diffusion on a surface.

This work was supported mainly by the U.S. Department of Energy (DOE), Office of Science, Basic Energy Sciences, Materials Sciences and Engineering Division. This includes the contributions by Y.H. and M.C.T. Research was performed at the Ames Laboratory, which is operated by Iowa State University under Contract No. DE-AC02-07CH11358. J.W.E. was supported for this work by NSF Grant No. CHE-1507223. DFT calculations were mainly performed with a grant of computer time at the National Energy Research Scientific Computing Centre (NERSC). NERSC is a DOE Office of Science User Facility supported by the Office of Science of the U.S. DOE under Contract No. DE-AC02-05CH11231. The calculations also partly used the Extreme Science and Engineering Discovery Environment (XSEDE), which is supported by National Science Foundation under Grant No. ACI-1548562. Y.H. thanks Graeme Henkelman for his help in the CINEB calculations.

## DATA AVAILABILITY

The data that support the findings of this study are available from the corresponding author upon reasonable request.

## REFERENCES

[1]M. S. Stark, K. L. Kuntz, S. J. Martens, and S. C. Warren, Adv. Mater. **31**, 1808213 (2019).
[2]L. Daukiya, M. N. Nair, M. Cranney, F. Vonau, S. Hajjar-Garreau, D. Aubel, and L. Simon, Prog. Surf. Sci. **94**, 1 (2019).
[3]J. Wan, S. D. Lacey, J. Dai, W. Bao, M. S. Fuhrer, and L. Hu, Chem. Soc. Rev. **45**, 6742 (2016).
[4]N. Briggs, Z. M. Gebeyehu, A. Vera, T. Zhao, K. Wang, A. D. L. F. Duran, B. Bersch, T. Bowen, K. L. Knappenberger, and J. A. Robinson, Nanoscale **11**, 15440 (2019).
[5]C. Riedl, C. Coletti, T. Iwasaki, A. A. Zakharov, and U. Starke, Phys. Rev. Lett. **103**, 246804 (2009).
[6]I. Gierz, T. Suzuki, R. T. Weitz, D. S. Lee, B. Krauss, C. Riedl, U. Starke, H. Höchst, J. H. Smet, C. R. Ast, and K. Kern, Phys. Rev. B **81**, 235408 (2010).
[7]S. Oida, F. R. McFeely, J. B. Hannon, R. M. Tromp, M. Copel, Z. Chen, Y. Sun, D. B. Farmer, and J. Yurkas, Phys. Rev. B **82**, 041411 (2010).
[8]S. L. Wong, H. Huang, Y. Wang, L. Cao, D. Qi, I. Santoso, W. Chen, and A. T. S. Wee, ACS Nano **5**, 7662 (2011).
[9]J. Sforzini, L. Nemec, T. Denig, B. Stadtmüller, T.-L. Lee, C. Kumpf, S. Soubatch, U. Starke, P. Rinke, V. Blum, F. C. Bocquet, and F. S. Tautz, Phys. Rev. Lett. **114**, 106804 (2015).
[10]J. L. McChesney, A. Bostwick, T. Ohta, T. Seyller, K. Horn, J. González, and E. Rotenberg, Phys. Rev. Lett. **104**, 136803 (2010).
[11]K. Kanetani, K. Sugawara, T. Sato, R. Shimizu, K. Iwaya, T. Hitosugi, and T. Takahashi, Proc. Natl. Acad. Sci. U. S. A. **109**, 19610 (2012).
[12]K. Li, X. Feng, W. Zhang, Y. Ou, L. Chen, K. He, L.-L. Wang, L. Guo, G. Liu, Q.-K. Xue, and X. Ma, Appl. Phys. Lett. **103**, 062601 (2013).
[13]R. Shimizu, K. Sugawara, K. Kanetani, K. Iwaya, T. Sato, T. Takahashi, and T. Hitosugi, Phys. Rev. Lett. **114**, 146103 (2015).
[14]S. Ichinokura, K. Sugawara, A. Takayama, T. Takahashi, and S. Hasegawa, ACS Nano **10**, 2761 (2016).
[15]B. M. Ludbrook, G. Levy, P. Nigge, M. Zonno, M. Schneider, D. J. Dvorak, C. N. Veenstra, S. Zhdanovich, D. Wong, P. Dosanjh, C. Straßer, A. Stöhr, S. Forti, C. R. Ast, U. Starke, and A. Damascelli, Proc. Natl. Acad. Sci. U. S. A. **112**, 11795 (2015).
[16]J. A. Robinson, M. Hollander, M. LaBella, K. A. Trumbull, R. Cavalero, and D. W. Snyder, Nano Lett. **11**, 3875 (2011).
[17]S. Tanabe, M. Takamura, Y. Harada, H. Kageshima, and H. Hibino, Appl. Phys. Express **5**, 125101 (2012).
[18]S. Forti, A. Stöhr, A. A. Zakharov, C. Coletti, K. V. Emtsev, and U. Starke, 2D Mater. **3**, 035003 (2016).

[19]M. Kim, M. C. Tringides, M. T. Hershberger, S. Chen, M. Hupalo, P. A. Thiel, C.-Z. Wang, and K.-M. Ho, Carbon **123**, 93 (2017).
[20]P. Rosenzweig, H. Karakachian, S. Link, K. Küster, and U. Starke, Phys. Rev. B **100**, 035445 (2019).
[21]H. Kim, O. Dugerjav, A. Lkhagvasuren, and J. M. Seo, Carbon **144**, 549 (2019).
[22]Y. R. Niu, A. A. Zakharov, and R. Yakimova, Ultramicroscopy **183**, 49 (2017).
[23]S. Forti, S. Link, A. Stöhr, Y. Niu, A. A. Zakharov, C. Coletti, and U. Starke, Nat. Commun. **11**, 2236 (2020).
[24]G. Henkelman and H. Jónsson, J. Chem. Phys. **113**, 9978 (2000).
[25]D. W. Boukhvalov and C. Virojanadara, Nanoscale **4**, 1749 (2012).
[26]N. A. Anderson, M. Hupalo, D. Keavney, M. Tringides, and D. Vaknin, J. Magn. Magn. Mater. **474**, 666 (2019).
[27]C. Virojanadara, A. A. Zakharov, R. Yakimova, and L. I. Johansson, Surf. Sci. **604**, L4 (2010).
[28]S. Watcharinyanon, C. Virojanadara, J. R. Osiecki, A. A. Zakharov, R. Yakimova, R. I. G. Uhrberg, and L. I. Johansson, Surf. Sci. **605**, 1662 (2011).
[29]F. Speck, J. Jobst, F. Fromm, M. Ostler, D. Waldmann, M. Hundhausen, H. B. Weber, and T. Seyller, Appl. Phys. Lett. **99**, 122106 (2011).
[30]A. Markevich, R. Jones, S. Öberg, M. J. Rayson, J. P. Goss, and P. R. Briddon, Phys. Rev. B **86**, 045453 (2012).
[31]J. D. Emery, V. D. Wheeler, J. E. Johns, M. E. McBriarty, B. Detlefs, M. C. Hersam, D. K. Gaskill, and M. J. Bedzyk, Appl. Phys. Lett. **105**, 161602 (2014).
[32]G. Sclauzero and A. Pasquarello, Appl. Surf. Sci. **291**, 64 (2014).
[33]Y.-P. Lin, Y. Ksari, and J.-M. Themlin, Nano Res. **8**, 839 (2015).
[34]J. Kunc, M. Rejhon, and P. Hlídek, AIP Adv. **8**, 045015 (2018).
[35]T. A. de Jong, E. E. Krasovskii, C. Ott, R. M. Tromp, S. J. van der Molen, and J. Jobst, Phys. Rev. Mater. **2**, 104005 (2018).
[36]I. Forbeaux, J.-M. Themlin, and J.-M. Debever, Phys. Rev. B **58**, 16396 (1998).
[37]T. Ohta, A. Bostwick, T. Seyller, K. Horn, and E. Rotenberg, Science **313**, 951 (2006).
[38]Y. Han, J. W. Evans, and M. C. Tringides, Phys. Rev. Materials **5**, 074004 (2021).
[39]A. Mattausch and O. Pankratov, Phys. Rev. Lett. **99**, 076802 (2007).
[40]S. J. Sung, J. W. Yang, P. R. Lee, J. G. Kim, M. T. Ryu, H. M. Park, G. Lee, C. C. Hwang, K. S. Kim, J. S. Kim, and J. W. Chung, Nanoscale **6**, 3824 (2014).
[41]F. Bisti, G. Profeta, H. Vita, M. Donarelli, F. Perrozzi, P. M. Sheverdyaeva, P. Moras, K. Horn, and L. Ottaviano, Phys. Rev. B **91**, 245411 (2015).
[42]N. M. Caffrey, R. Armiento, R. Yakimova, and I. A. Abrikosov, Phys. Rev. B **92**, 081409 (2015).
[43]M. Lorenzo, C. Escher, T. Latychevskaia, and H.-W. Fink, Nano Lett. **18**, 3421 (2018).
[44]W. Li, L. Huang, M. C. Tringides, J. W. Evans, and Y. Han, J. Phys. Chem. Lett. **11**, 9725 (2020).
[45]Y. Han, K. C. Lai, A. Lii-Rosales, M. C. Tringides, J. W. Evans, and P. A. Thiel, Surf. Sci. **685**, 48 (2019).
[46]B. Silvi and A. Savin, Nature **371**, 683 (1994).
[47]Y. Han, J. W. Evans, and M. C. Tringides, "Thermodynamics and kinetics of H adsorption and intercalation for graphene on 6H-SiC(0001) from first-principles calculations," J. Vac. Sci. Technol. A (to be published) (2021).
[48]T. E. Markland and M. Ceriotti, Nat. Rev. Chem. **2**, 0109 (2018).
[49]H. Kimizuka, S. Ogata, and M. Shiga, Phys. Rev. B **100**, 024104 (2019).
[50]Y. Shi, J. Qi, Y. Han, and T. Lu, Phys. Rev. Appl. **10**, 024021 (2018).